Enhanced FRONSAC Encoding with Compressed Sensing

Haifeng Wang[1], R. Todd Constable[1], and Gigi Galiana[1]
[1]*Yale University, New Haven, CT, United States*

Target Audience: Researchers interested in parallel or accelerated imaging, nonlinear gradient encoding, or compressed sensing

Purpose: Nonlinear spatial encoding magnetic (SEM) fields have been studied to reduce the number of echoes needed to reconstruct a high quality image, but optimal schemes are still unknown [1-8]. Last year, we showed that adding a rotating nonlinear field of modest amplitude, which we call the FRONSAC (Fast ROtary Nonlinear Spatial ACquisition) imaging [8], greatly improved images from highly undersampled conventional linear trajectories. Even weak FRONSAC fields significantly improved the images, but the strongest or highest frequency oscillating fields showed the most improvement on undersampled trajectories. However, since the ultimate goal is to acquire the trajectories in a single short TR, lower amplitude FRONSAC gradients are desirable for application constrains. FRONSAC creates undersampling artifacts that are relatively incoherent and well suited to compressed sensing (CS) reconstruction. CS is a sparsity-promoting convex algorithm to recon images from highly undersampled datasets [9-10]. In this paper, we present a hybrid, CS-FRONSAC, which combines these two methods. The results illustrate the proposed method improves incoherence between the sensing and sparse domains, and ultimately image quality compared with results recovered by the Kaczmarz algorithm [2]. The resulting improvement allows us to consider FRONSAC gradients with lower amplitudes and frequencies, further lowering hardware demands as well as the dB/dt burden.

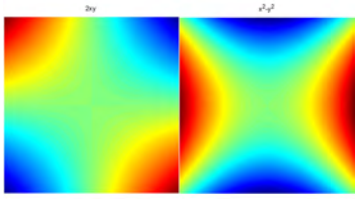

Fig. 1. Simulated nonlinear second-order spatial emcoding filed maps (2xy and x^2-y^2)

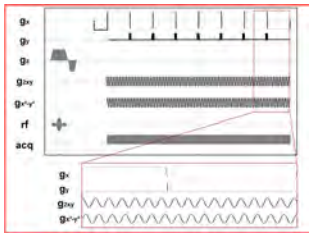

Fig. 2. Timing diagram of the FRONSAC EPI pulse

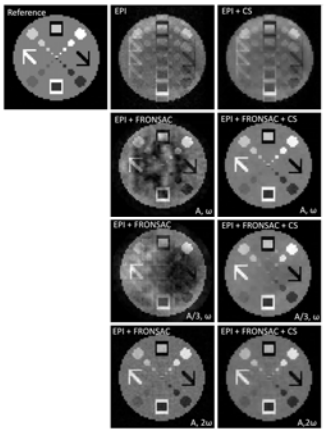

Fig. 3. Simulation results with the 64×64 resolution including reference, results in linear gradient fields (EPI), and nonlinear spatial encoding (FRONSAC and FRONSAC with CS)

Theory: Neglecting relaxation effects, the signal s_q from the q-th RF channel should satisfy $s_q = \int_\Omega m(\mathbf{x}) C_q(\mathbf{x}) e^{i\Phi(\mathbf{x},t)} d\mathbf{x}$, where $m(\mathbf{x})$ is the magnetization at location $\mathbf{x}$ = (x, y), $C_q(\mathbf{x})$ is the sensitivity of q-th coil, and the integral is over Ω, which is the region of interest; $\Phi(\mathbf{x}, t)$ is the spatially dependent encoding phase. Using the FRONSAC imaging fields (2xy and x^2-y^2, as seen as Fig. 1), $\Phi(\mathbf{x}, t)$ is $\Phi(\mathbf{x},t) = k_x(t)x + k_y(t)y + A\cdot\sin(\omega t)\cdot 2xy + A\cdot\cos(\omega t)\cdot(x^2 - y^2)$, where A is the maximum amplitude of the second-order gradient waveforms; $k_x(t)$ and $k_y(t)$ are vectors of gradient moments describing the evolution of each linear gradient field over time.

To further improve image quality, we replace our standard Kaczmarz reconstruction with a CS algorithm. As described in previous work [10] on CS reconstruction for O-Space, we apply the CS reconstruction with the encoding matrix, instead of the conventional Fourier encoding matrix **E**. This convex optimization may be written as: $\mathbf{f} = \arg\min\left\{\|\mathbf{Ef} - \mathbf{s}\|_2 + \lambda\|\Psi\mathbf{f}\|_1\right\}$ where, **f** is the desired image; **s** is the measured signal; $\|\cdot\|_2$ and $\|\cdot\|_1$ are L-2 and L-1 norm; **E** is the encoding matrix, i.e. measurement basis or sensing matrix, with its inverse calculated by the Kaczmarz iterative algebraic reconstruction, a pseudo-inverse algorithm to converge the minimum lease squares norm solution [2, 10]; Ψ is the sparsity transform, such as wavelet, contourlets, finite differences, etc.; λ is the relaxation parameter and is typically set for strongly under-relaxed reconstructions for gradual convergence.

Methods: All simulations were performed in MATLAB (MathWorks, Natick, MA, USA) with a 64^2 resolution. The base linear trajectory corresponds to an 8-fold undersampled EPI acquisition with total acquisition time of 25.6ms, and the FRONSAC gradients are applied as shown in Figure 2. Here, A and ω are respectively equal to A = 790 Hz/cm^2; $\omega/2\pi$ = 3.2kHz. Each readout samples 512 points per echo. Simulated receiver coil sensitivity profiles are from an 8 element array with noise of 5% maximum density. CS reconstruction was performed using wavelets as the basis in which we promote sparsity.

Results: Simulation results with the geometric phantom are shown in Fig. 3. The first row shows the reference object and reconstructions from an undersampled EPI acquisition (no FRONSAC gradient) using Kaczmarz (column 2) or a CS algorithm (column 3). The next row shows reconstructions from data simulated with an additional FRONSAC gradient applied with a strength corresponding to 790Hz/cm^2 and $\omega/2\pi$ = 3.2kHz. Though this FRONSAC gradient does not oscillate with sufficient frequency to remove all the undersampling artifacts, a standard iterative reconstruction (left image) yields more distributed undersampling artifacts than those observed in the absence of the FRONSAC gradient. Adding a sparsifying penalty (right image) greatly improves the image quality. The third row shows that CS reconstruction allows for still lower amplitude FRONSAC gradients (A/3). Finally, we show that even with low FRONSAC gradient strengths and rotation speeds (A and 2ω) which yield highly improved images without CS reconstruction, the additional sparsifying penalty improves the final result. These results illustrate that CS dramatically improves the image quality of FRONSAC encoded data.

Discussion and Conclusion: CS can improve image quality when combined with FRONSAC imaging. The findings illustrate that FRONSAC with small encoding gradients and smaller PNS burdens, can lead to shorter acquisition times. Stronger FRONSAC gradients allow high quality images from still fewer echoes.

References: **1**. Hennig et al. MAGMA. 21(1-2): 5-14, 2008; **2**. Stockmann et al. MRM. 64(2): 447-456, 2010; **3**. Tam et al. MRM. 69(4): 1166-1175, 2012; **4**. Gallichan et al. MAGMA. 25(6): 419-431, 2012; **5**. Galiana et al. PLoS One, 9(5): e86008, 2014; **6**. Testud et al. ISMRM. 2663, 2013; **7**. Littin et al. ISMRM. 2379, 2013; **8**. Layton et al. MRM. 70(3): 684-696, 2012; **8**. Wang et al. ISMRM. 4244, 2014; **9**. Lustig et al. MRM. 58(6): 1182-1195, 2007; **10**. Tam et al. MRM. doi: 10.1002/mrm.25364, 2014.